25th ABCM International Congress of Mechanical Engineering
October 20-25, 2019, Uberlândia, MG, Brazil

COB-2019-0053
ENERGY EFFICIENCY ANALYSIS OF SOLAR WATER HEATING SYSTEMS COMBINED WITH HEAT PUMPS

Valquíria Bomfim Fernandes
Gabriel Ivan Medina Tapia
Federal University of Rio Grande do Norte, Technology Center - Natal
valbfernandes@gmail.com, gmedinat@ct.ufrn.br

Abstract. *This work analyzes the performance of solar water heating systems, applied to large scale domestic consumption in the city of Natal-RN, Brazil. This analysis aims to stimulate the harnessing of solar resource as thermal energy, as a sustainable alternative to electric heating. Two conventional configurations are studied, as well as two configurations combined with heat pumps. The first conventional system contains a single storage tank, whose volume varies according to the area of installed solar collectors, whereas the other three systems have two storage tanks with fixed volume. The combined systems differ from each other in that one of them uses an air-to-water heat pump as an auxiliary heater, while the other relies on a water-to-water heat pump and a bypass valve to connect its two storage tanks. Weather data pertaining to the studied location is implemented in the format of a typical meteorological year (TMY). A methodology for mathematical modeling and transient numerical simulation is applied using the MATLAB software. According to the results, all configurations analyzed in this work prove advantageous. For applications with a reduced area of solar collectors, the combined systems are more effective, whereas the conventional systems show the best performance in cases where a larger area of collectors may be installed.*

Keywords: *water heating, heat pumps, combined systems, solar thermal energy*

1. INTRODUCTION

The use of electric showers for domestic water heating represents a large part of the residential electricity consumption in Brazil, amounting to 24% of the national total. While this use is reduced in the Northeastern region, composing 9% of local consumption, it is still a significant contributor to the peak of electricity demand between the hours of 17h and 21h. (PROCEL, 2007). A more environmentally sustainable and economically viable alternative, according to Naspolini (2012), appears in the form of solar water heating, which harnesses the already available solar radiation. Another option is presented in the form of heat pumps, with a high energy efficiency. As proposed by Gonçalves (2016), it is possible to associate both options into solar water heating systems combined with heat pumps, in order to increase the amount of energy obtained from solar collectors, as well as complement it.

This work aims to analyze the performance of solar water heating systems, both in conventional configurations and combined to heat pumps, applied to large scale domestic consumption in the city of Natal - RN. The methodology used consists of a mathematical modeling of the systems and their components, coupled with transient numerical simulations for a typical meteorological year (TMY). An energy efficiency analysis is made, using the Free Energy Fraction (FEF) as parameter, as well as the fractions of demand for the auxiliary heater and the heat pumps.

2. SYSTEMS DESCRIPTION

Four systems are analyzed in this work, as proposed by Gonçalves (2016): two conventional solar water heating systems, which serve as a basis of comparison, and two solar water heating systems combined with heat pumps. All configurations are composed of a series array of flat plate solar thermal collectors, connected to a thermal storage tank (ST). Additionally, all systems are equipped with an auxiliary gas heater (AUX), connected to the top portion of the thermal storage. The inlet and outlet of water to the system is regulated by mixing and thermostatic valves. The first configuration is shown in Fig. 1, for the Conventional System 1. The volume of the single storage tank is set to vary according to the size of the collector array.

Figure 2 shows Conventional System 2, which adds a second thermal storage tank, ST2, connected in series to the first storage tank, ST1. The aim of this separation is to reduce the heat transfer due to mixing water at a lower temperature from the inlet with water kept at a higher temperature by the auxiliary heater. For this and the following systems, both tanks have fixed volumes regardless of the area of collectors.

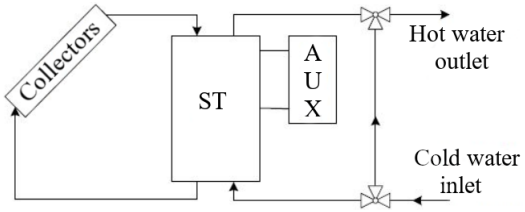

Figure 1: Simplified schematics of Conventional System 1. Adapted from Gonçalves, 2016.

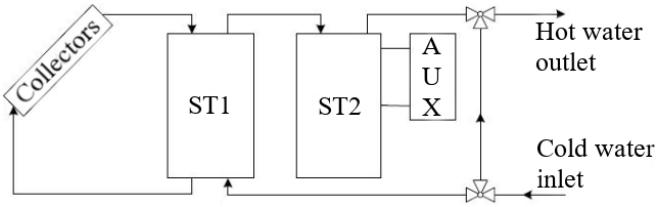

Figure 2: Simplified schematics of Conventional System 2. Adapted from Gonçalves (2016).

Next, Fig. 3 shows the elements of the Air Source Heat Pump (ASHP) System. This configuration adds a heat pump, HP, as an auxiliary heater, which transfers heat from the ambient air into the water in ST2.

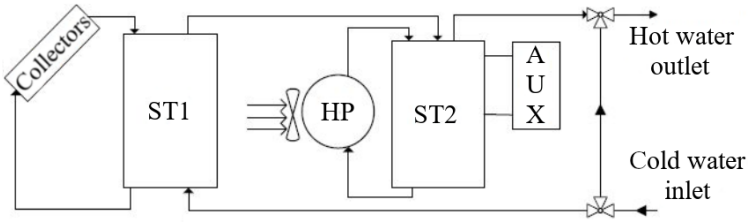

Figure 3: Simplified schematics of the Air Source Heat Pump (ASHP) System. Adapted from Gonçalves (2016).

Lastly, Fig. 4 presents the schematics for the Water Source Heat Pump (WSHP) System, which connects ST1 and ST2 with a heat pump, HP, in parallel to a bypass valve. This heat pump transfers heat from the water in ST1 to the water in ST2, aiming to increase the efficiency and operating time of the collectors. The system is modeled according to Sterling (2011), except for the replacement of the heat exchanger with a bypass valve, as proposed by Gonçalves (2016).

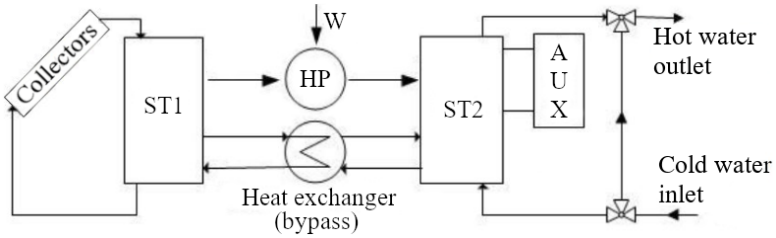

Figure 4: Simplified schematics of the Water Source Heat Pump (WSHP) System. Adapted from Gonçalves (2016).

3. COMPONENT MATHEMATICAL MODELS

The system components were modeled mathematically as follows, and a yearly simulation of each system was implemented on MATLAB. The differential equations for water temperature were solved for every hour using the one-dimensional finite-differences method.

3.1 Meteorological data

The weather data for the city of Natal was obtained from the SWERA (Solar Wind and Energy Resource Assessment) national database, provided in the format of a typical meteorological year (TMY), as recommended by Cardemil and Colle (2010). The file contains hourly values for the beam solar radiation on a horizontal surface, I_b, the diffuse horizontal radiation, I_d, and the total radiation on a horizontal surface, I, as well as ambient temperature, T_{amb}, and the air's wet-bulb temperature (Gonçalves, 2016). This data was processed into the solar radiation incident on the solar collector surface, I_T, using the Perez Anisotropic Sky Model according to Duffie and Beckman (2006), as seen in Eq. (1):

$$I_T = I_b R_b + I_d(1 - F_1)\left(\frac{1 + \cos\beta}{2}\right) + I_d F_1 \frac{a}{b} + I_d F_2 \sin\beta + I\rho_g\left(\frac{1 - \cos\beta}{2}\right), \tag{1}$$

in which ρ_g is the surface albedo of the surroundings, β is the slope of the flat plate collector, F_1 and F_2 are luminosity coefficients (Duffie and Beckman, 2006) and R_b is the ratio presented in Eq. (2):

$$R_b = \frac{\cos\theta}{\cos\theta_z}, \tag{2}$$

in which θ is the angle of incidence of beam radiation and θ_z is the zenith angle. Lastly for Eq. (1), the term a is defined as $a = \cos\theta$, if this is a positive value, or $a = 0$ otherwise, while b is defined as either $b = \cos\theta_z$ or $b = \cos 85°$, depending on whichever value is greater.

3.2 Solar flat plate collector

The solar collector receives as input the inlet water temperature, $T_{c,in}$, considered equal to the wet-bulb temperature from the weather data, as well as the values for I_T and T_{amb} from the previous component. The total area of collectors, A_c, is set for each yearly simulation, and the mass-flow of water through the collector, $\dot{m}_c$, varies according to the hourly consumption of hot water. The basic equations for this component were defined according to Gonçalves (2016), starting with the rate of useful heat transfer, $\dot{Q}_u$, in Eq. (3):

$$\dot{Q}_u = \dot{m}_c c_p (T_{c,o} - T_{c,i}), \tag{3}$$

in which c_p is the water's specific heat and $T_{c,out}$ is its outlet temperature. The instant efficiency of the solar collector, η_c, expresses its capacity to absorb the incident radiation I_T, and is given by Eq. (4), adapted from the Hottel-Whillier equation (Duffie and Beckman, 2006):

$$\eta_c = a_0 - a_1 \frac{\Delta T}{I_T}, \tag{4}$$

in which $\Delta T = T_{c,in} - T_{amb}$. The values for $a_0 = F_R(\tau\alpha)_n$ and $a_1 = F_R U_L$ are provided by the manufacturer's catalog. The term F_R is the heat removal factor of the fluid, $(\tau\alpha)_n$ is the transmittance-absorptance product of the collector for beam radiation, and U_L is the modified heat loss coefficient for the collector, provided by the manufacturer's catalog (TOSI Ltda) as constant.

The former equations consider the collector operating under ideal test conditions, which often differ from the actual operating conditions. Therefore, correction factors must be applied to account for the three main variations (Gonçalves, 2016). First, an incidence angle modifier, $K_{\tau\alpha}$, corrects for the varying angles of incident solar radiation throughout the day. $K_{\tau\alpha}$ is described by Eq. (5):

$$K_{\tau\alpha} = 1 - b_0\left(\frac{1}{\cos\theta} - 1\right) - b_1\left(\frac{1}{\cos\theta} - 1\right)^2, \tag{5}$$

where b_0 and b_1 are given by the manufacturer's catalog. Next, the flow rate correction factor r_1 considers the use of the collector at a flow rate other than that of the test conditions, and is defined by Eq. (6) (Duffie and Beckman, 2006):

$$r_1 = \frac{\left(\frac{\dot{m}_c c_p}{A_c F' U_L}\right)_{use}\left[1 - exp\left(\frac{-A_c F' U_L}{\dot{m}_c c_p}\right)\right]_{use}}{\left(\frac{\dot{m}_c c_p}{A_c F' U_L}\right)_{test}\left[1 - exp\left(\frac{-A_c F' U_L}{\dot{m}_c c_p}\right)\right]_{test}}, \tag{6}$$

in which $F'U_L$ is calculated for test conditions through Eq. (7):

$$F'U_L = -\frac{\dot{m}_c c_p}{A_c}\log\left(1 - \frac{A_c F_R U_L}{\dot{m}_c c_p}\right). \tag{7}$$

The third correction factor, r_2, accounts for the simplification of a series array as a single collector, and is described by Eq. (8), in which N_S is the number of collectors, and the test flow rate is used for $\dot{m}_c$.

$$r_2 = \frac{1 - \left(1 - \frac{A_c F_R U_L}{\dot{m}_c c_p}\right)^{N_S}}{N_S \frac{A_c F_R U_L}{\dot{m}_c c_p}}. \tag{8}$$

Thus, the corrected equation for useful heat rate is given by Eq. (9),

$$\dot{Q}_u = \eta_c A_c I_T = r_1 r_2 A_c [I_T K_{\tau\alpha} a_0 - a_1 \Delta T], \tag{9}$$

which is combined with Eq. (3) to give the outlet temperature of the collector as:

$$T_{c,out} = T_{c,in} + \frac{r_1 r_2 A_c}{\dot{m}_c c_p} [I_T K_{\tau\alpha} a_0 - a_1 \Delta T]. \tag{10}$$

3.3 Thermal storage tank

The model used is based on the equations set by Duffie and Beckman (2006) for a vertical cylindrical tank with constant volume, divided into isothermic nodes to simulate the phenomenon of temperature stratification. An energy balance equation is solved for each node, accounting for three forms of heat transfer: conduction, natural convection due to the temperature difference between nodes, and forced convection due to the mass flows entering and leaving the tank. The model is considered to have fixed outlets and variable inlets, an auxiliary heater attached to the upper node, and a total of five nodes. For a node i, of mass m_i, the instant temperature, $T_{s,i}$, is given by an energy balance accounting for the heat rates entering and leaving the node, as seen in Eq. (11):

$$\frac{dT_{s,i}}{dt} = \frac{\dot{Q}_{aux,i} - \dot{Q}_{loss,i} - \dot{Q}_{cond,i} - \dot{Q}_{flow,i} - \dot{Q}_{mix,i}}{m_i c_p}, \tag{11}$$

where $\dot{Q}_{aux,i}$ is the heat rate supplied by the auxiliary heater, $\dot{Q}_{loss,i}$ is the heat loss rate to the environment through the walls of the tank, $\dot{Q}_{cond,i}$ is the heat rate transferred to and from the adjacent nodes through conduction, $\dot{Q}_{flow,i}$ is the heat rate transferred to and from adjacent nodes through forced convection (due to mass flow entering and leaving the tank), and $\dot{Q}_{mix,i}$ is the heat rate spent mixing nodes in order to stabilize the temperature differences in the model (Gonçalves, 2016).

The terms $\dot{Q}_{loss,i}$ and $\dot{Q}_{cond,i}$ are defined according to Gonçalves (2016), whereas $\dot{Q}_{flow,i}$ and $\dot{Q}_{mix,i}$ require control functions, for the mass flow entering or leaving the node (Duffie and Beckman, 2006). Equation (12) shows the control functions $F_{h,i}$ for a hot water flow entering at node i:

$$F_{h,i} = \begin{cases} 1 \text{ if } i = 1 \text{ and } T_{in} > T_{s,i} \\ 1 \text{ if } T_{s,i-1} \geq T_{in} > T_{s,i} \\ 0 \text{ for any other case} \end{cases}, \tag{12}$$

so that the function returns 1 (true) if the temperature of the incoming flow, T_{in}, is greater than that of the node in question, $T_{s,i}$, yet smaller than the temperatur at the node directly above, $T_{s,i-1}$. Similarly, for a colder influx of water Eq. (13) shows $F_{c,i}$:

$$F_{c,i} = \begin{cases} 1 \text{ if } i = N_S \text{ and } T_{in} < T_{s,N_S} \\ 1 \text{ if } T_{s,i-1} \geq T_{in} > T_{s,i} \\ 0 \text{ for any other case} \end{cases}, \tag{13}$$

which returns true in case the temperature of the incoming flow is inferior to $T_{s,i-1}$. Then, a function for the total mass flow entering a node i, $\dot{m}_{f,i}$, is defined by Eq. (14):

$$\dot{m}_{f,i} = \dot{m}_{in,hot} \sum_{j=1}^{i-1} F_{h,j} - \dot{m}_{in,cold} \sum_{j=i+1}^{N_s} F_{c,j}, \tag{14}$$

which gives Eq. (15) for heat rate transferred due to forced convection:

$$\dot{Q}_{flow,i} = F_{h,i}\dot{m}_{in,hot}(T_{in} - T_{s,i}) + F_{c,i}\dot{m}_{in}(T_{in} - T_{s,i}) + \begin{cases} \dot{m}_{f,i}(T_{s,i-1} - T_{s,i}) & \text{if } \dot{m}_{f,i} > 0 \\ \dot{m}_{f,i+1}(T_{s,i} - T_{s,i+1}) & \text{if } \dot{m}_{f,i+1} < 0 \end{cases}, \quad (15)$$

in which the first two terms account for mass flow directly entering node i, and the terms in brackets refer to mass flow coming from adjacent nodes, either above $(i-1)$ or below $(i+1)$.

The effects of mixture between nodes due to eventual destratification, $\dot{Q}_{mix,i}$, is represented by Eq. (16):

$$\dot{Q}_{mix,i} = \dot{m}_m c_p [F_{m,a,i}(T_{s,i-1} - T_{s,i}) + F_{m,b,i}(T_{s,i+1} - T_{s,i})], \quad (16)$$

where $\dot{m}_m$ is the mixture mass flow, and the control functions for mixture with the node above, $F_{m,a,i}$, and with the node below $F_{m,b,i}$ are defined by Eq. (17) and Eq. (18), respectively, in which ΔT_{max} is the maximum temperature difference between nodes:

$$F_{m,a,i} = \begin{cases} 1 \text{ if } i > 1 \text{ and } T_{s,i-1} > \Delta T_{max} \\ 0 \text{ for any other case} \end{cases}, \quad (17)$$

$$F_{m,b,i} = \begin{cases} 1 \text{ if } i < N_S \text{ and } (T_{s,i} - T_{s,i+1}) > \Delta T_{max} \\ 0 \text{ for any other case} \end{cases}, \quad (18)$$

3.4 Heat pumps

The air source heat pump (ASHP) and the water source heat pump (WSHP) were modeled using data from the manufacturer's catalogs for heat rate capacity, $\dot{Q}_{hp}$, power consumption of the heat pump, $\dot{W}_{hp}$, and coefficient of performance, COP, related as defined by Eq. (19).

$$\dot{Q}_{hp} = \dot{W}_{hp} \cdot COP. \quad (19)$$

Additionally, COP is considered to vary according to the temperature of the heat source, which is the ambient air temperature, T_{amb}, for ASHP, and the inlet temperature from the cold water reservoir, $T_{cold,in}$, for WSHP. For ASHP, two performance curves were obtained from the literature (Welch, 2010) for water leaving the heat pump at 35 °C and 50 °C. The data was then interpolated to generate a new curve, for water leaving at 45 °C, consistent with the catalog data used in this work, as shown in Fig. 5. The new linearized curve y corresponds to Eq. (20). As for the water source heat pump, catalog data was provided for performance at different water temperatures, for the test volume flow rate, so that a curve was similarly obtained for the variation of COP according to $T_{cold,in}$, as seen in Fig. 6. This linearized curve corresponds to Eq. (21). Both curves showed regression coefficients, R, approximate to one, indicating they accurately describe the interpolated data.

$$COP_{ASHP} = 0.0637 \cdot T_{amb} + 2.69, \quad (20)$$

$$COP_{WSHP} = 0.0514 \cdot T_{cold,in} + 3.37, \quad (21)$$

which can be combined with Eq. (19) to obtain $\dot{Q}_{hp}$. Then, the water temperature at either heat pump's outlet to the hot reservoir, $T_{hp,out}$ can be obtained from Eq. (22) (Gonçalves, 2016):

$$T_{hp,out} = T_{hp,in} + \frac{\dot{Q}_{hp}}{\dot{m}_{hp} c_p}, \quad (22)$$

in which $T_{hp,in}$ is the water temperature at the heat pump's inlet, and $\dot{m}_{hp}$ is the mass flow of water through the heat pump, also provided by the catalog.

Lastly, the heat rate obtained from the environment in the evaporator of the heat pump, $\dot{Q}_{hp,evap}$, can be obtained by applying an energy balance equation to the heat pump (Gonçalves, 2016), summarized by Eq. (23):

$$\dot{Q}_{hp,evap} = \dot{Q}_{hp} - \dot{W}_{hp}. \quad (23)$$

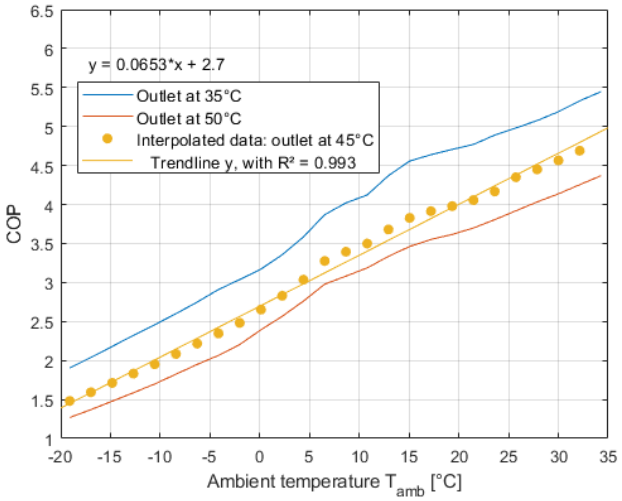

Figure 5: ASHP performances for different outlet water temperatures. Adapted from Welch (2010).

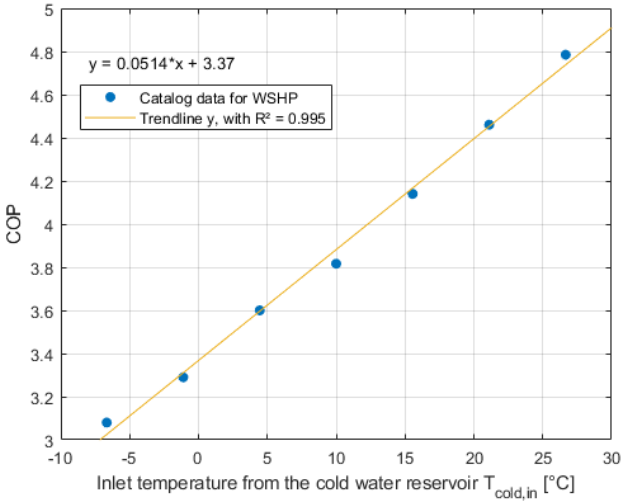

Figure 6: WSHP performances for a test volume flow rate of 6 gpm or 3.76×10^{-4} m^3/s.

3.5 Hot water consumption profile

The pattern of hourly domestic hot water consumption used in this work follows the profile seen in Fig. 7, established by Salazar (1997) for the city of Florianópolis, Brazil, and for a total daily consumption of 150 liters. This profile was scaled upwards to a daily total of 20000 liters to account for a large-scale demand, such as that of a residential building, according to Gonçalves (2016).

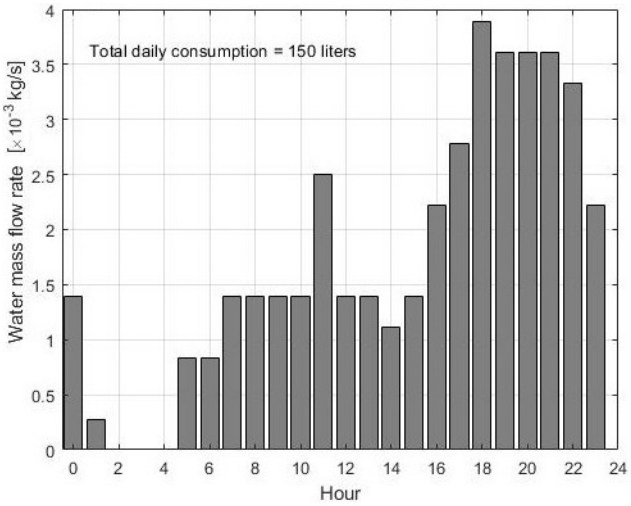

Figure 7: Domestic hot water consumption profile. Adapted from Salazar (1997).

3.6 Energy efficiency indicators

The energy efficiency of the proposed systems is evaluated using the Free Energy Fraction (FEF), as defined by Freeman *et al.* (1979). The total energy delivered by each system is represented by the heat rate delivered as hot water, $\dot{Q}_{DHW}$, integrated over the total time period analyzed. The FEF is then the fraction of this energy which was obtained from the environment, either from solar radiation captured by the flat plate collectors, or from the ambient air, extracted using the heat pump. Thus, the value of FEF indicates the fraction of energy saved by a system, and is defined by Eq. (24):

$$FEF = \frac{\int(\dot{Q}_u + \dot{Q}_{hp,evap})dt}{\int \dot{Q}_{DHW}dt}. \tag{24}$$

Additionally, the fraction of demand for the heat pump, $F_{d,hp}$, represents the ratio of heat supplied by the condenser of the heat pump, in relation to the total energy delivered as hot water, as seen in Eq. (25). Lastly, the fraction of demand

for the auxiliary heater, $F_{d,aux}$, is defined as the fraction of the total energy delivered which was provided by the auxiliary heater, as an integration of its power, P_{aux}, over the total time period analyzed, as seen in Eq. (26).

$$F_{d,hp} = \frac{\int \dot{Q}_{hp} dt}{\int \dot{Q}_{DHW} dt}. \tag{25}$$

$$F_{d,aux} = \frac{\int P_{aux} dt}{\int \dot{Q}_{DHW} dt}. \tag{26}$$

4. SIMULATION PARAMETERS

The systems were simulated for a full meteorological year, initiating with the input of meteorological data, in order to calculate the incident radiation on the solar collectors throughout the year. Then, a time loop is initiated to model the systems' operation in an hourly basis. Each system component requires particular parameters, detailed as follows.

4.1 General parameters

The general parameters seen in Tab. 1 refer to the total simulation time, time step size and latitude of the location studied, in this case the city of Natal - RN, Brazil. The solution method for differential equations was that of finite-difference equations, discretized via the explicit method. Additionally, the surface albedo of the surroundings was considered as $\rho_g = 0.2$, equivalent to a dry concrete surface (Feister and Grewe, 1995). Water specific heat and thermal conductivity were obtained for water at 40 °C, as $c_p = 4178$ J/(kg.K) and $k_w = 0.628$ W/(m.K), respectively.

Table 1: General parameters for the simulations.

Parameter	Value	Unit
Initial - final time	0 - 8760	hours
Time step size	0.04	hours
Location latitude	-5.812757	° (degrees)

4.2 Solar collector

Performance data for the solar collectors is taken from the TOSI Ltda. catalog for the collector model JFS 10, of the Jelly Fish line, with an estimated energy production of 89,51 kWh per month, and categorized as class A by the Inmetro energy efficiency table. The values of coefficients a_0, a_1, b_0 and b_1, as well as the mass flow per area used in laboratory tests, $\dot{m}''_{test}$, were provided in the catalog and can be seen in Tab. 2. Additionally, the table also contains the values defined for the positioning of the collector and the total area installed, which was simulated as variable.

Table 2: Solar collector parameters.

Parameter	Symbol	Value	Unit
Linear coefficient of the efficiency curve	a_0	0.77	-
Angular coefficient of the efficiency curve	a_1	4.27	W/(m^2.K)
Test mass flow per area of collectors	$\dot{m}''_{test}$	70.0	kg/(m^2.h)
First order coefficient for the incidence angle modifier	b_0	0.1065	-
Second order coefficient for the incidence angle modifier	b_1	0	-
Collector's slope relative to a horizontal surface	β	15	° (degrees)
Azimuth angle of the collector	γ	-135	° (degrees)
Area of collectors, variable	A_c	50 - 500	m^2

The inclination angle, β, was defined as approximately the absolute value of the local latitude, plus $10°$, and the azimuth angle, γ, was set to point northeast, so as to better absorb solar incidence in the morning hours, from the east, while also partially pointing towards the north, which receives the most solar radiation throughout the day in the Southern Hemisphere. Lastly, the area of installed solar collectors was set to vary within a range, and for each value of A_c analyzed, a full meteorological year was simulated. The values of that range were defined according to Gonçalves (2016), considering a minimum of 50 m^2 of collectors as necessary to ensure adequate operating conditions for the heat pump, and a maximum of 500 m^2 as an exaggerated upper limit, meant to approximate the results of an infinite area of collectors.

4.3 Thermal storage tanks

For the Conventional System 1, the thermal storage volume V_{ST} is contained within a single storage tank, whose volume is set to vary according to the size of the collector array, with 75 liters (0.075 m^3) of storage for every square meter of collectors, as recommended by Duffie and Beckman (2006). All other system contain two storage tanks with fixed volumes. The first tank has a volume of $V_{ST1} = 15$ m^3, while the second tank contains $V_{ST2} = 5$ m^3.

The geometric parameters of all storage tanks in this work are dependant on their volume, generically referred to as V_s. All thermal storage tanks maintain the same proportion ratio, S_s, as seen in Tab.3. Additionally, the thermal insulation on the tank walls was regarded as a layer of glass wool, with a thermal conductivity of 0.036 W/(m.K) and a thickness of 5 mm (Gonçalves, 2016).

Table 3: Geometric parameters of the thermal storage tanks. Gonçalves (2016).

Parameter	Symbol	Value	Unit
Proportion ratio of the storage tank	S_s	$D_s/H_s = 1/3$	-
Diameter of the storage tank	D_s	$(4 \cdot S_s V_s/\pi)^{1/3}$	m
Height of the storage tank	H_s	D_s/S_s	m

Lastly, the parameters for the mixing between nodes are defined, which limit stratification. The Conventional System was considered capable of sustaining greater amounts of stratification, since its storage volume varies with the area of installed solar collectors, A_c. Therefore, the maximum temperature difference between nodes, ΔT_{max}, was set to also vary according to the total storage volume. The mixing mass flow rate, $\dot{m}_m$, was defined as corresponding to a quarter of the mass of one node, m_i, divided by an hour, for the lowest value of storage volume. Therefore, $\dot{m}_m = 0.25 \cdot m_{i,min}/(3600\ s)$.

As for the ASHP System, each storage tank is considered separately. The first tank, ST1, was considered more susceptible to destratification, due to its fixed volume being relatively small compared to the mass flow rate circulating to and from the solar collector, $\dot{m}_c$. This effect becomes more pronounced as A_c increases, resulting in higher water temperatures at the collector outlet. Therefore, ΔT_{max} is limited and $\dot{m}_m = 2 \cdot m_i/(3600\ s)$ for ST1. The second storage tank, ST2, has lower mass flow rates enter and leave it, and so its mixing mass flow rate is simply $\dot{m}_m = 0.25 \cdot m_i/(3600\ s)$. Table 4 summarizes the parameters described above.

Table 4: Mixing parameters of the thermal storage tanks.

System	Storage tank	Maximum temperature difference, ΔT_{max} [°C]	Mixing mass flow rate, $\dot{m}_m$ [kg/s]
Conventional 1	ST	$15 + 20\left(\frac{V_s - V_{s,min}}{V_{s,max} - V_{s,min}}\right)$	0.0518
Conventional 2, ASHP and WSHP	ST1	10	2.4875
	ST2	15	0.0691

4.4 Heat pumps

The catalog data used to simulate the operation of the air source heat pump in the ASHP System correspond to that of the air-to-water heat pump model 30RQSY 039, of Carrier's Aquasnap series. This equipment operates using the refrigerant R-410A and is composed of a plate heat exchanger as a condenser, a finned evaporator with copper tubes and aluminum fins, a scroll compressor and an axial fan.

Table 5: Nominal characteristics of the air source and water source heat pumps.

Heat pump	COP	Nominal heat rate capacity $\dot{Q}_{nom}$ [kW]	Inlet temperature [°C]	
ASHP	3.16	42.0	Cold reservoir (air)	-20 to 35
			Hot reservoir (water)	25 to 55
WSHP	4.4	9.08	Cold reservoir (water)	-6 to 26
			Hot reservoir (water)	21 to 43

The data used for the water source heat pump in the WSHP System was obtained from the catalog of the water-to-water

heat pump model 50PSW025, of Carrier's Aquazone series, which also uses the refrigerant R-410A and is composed of scroll compressors, two double pipe heat exchangers and a thermal expansion valve. The nominal heat rate capacity, performance coefficient and operating temperature range for both equipments can be seen in Tab. 5.

The heat rate capacity for the simulation, $\dot{Q}_{sim}$, was scaled down for ASHP by multiplying the nominal value by a scale factor, FE = 0.3, so that $\dot{Q}_{sim} = FE \cdot \dot{Q}_{nom}$. This way, the catalog data was used to simulate a heat pump with a reduced capacity, similar to that of WSHP, for easier comparison between the two (Gonçalves, 2016).

5. RESULTS AND DISCUSSION

The results of energy efficiency for all systems are presented in the following graphs, as varying along the range of installed collector area simulated. Figure 8 shows the results of Free Energy Fraction, FEF, for which the ASHP System presents the highest values for collector areas between 50 and 100 m^2, with an initial FEF value of 0.57, significantly above that of the other systems. The WSHP System shows the best performance for areas between 100 and 150 m^2, after which it presents the lowest values of FEF among all four systems.

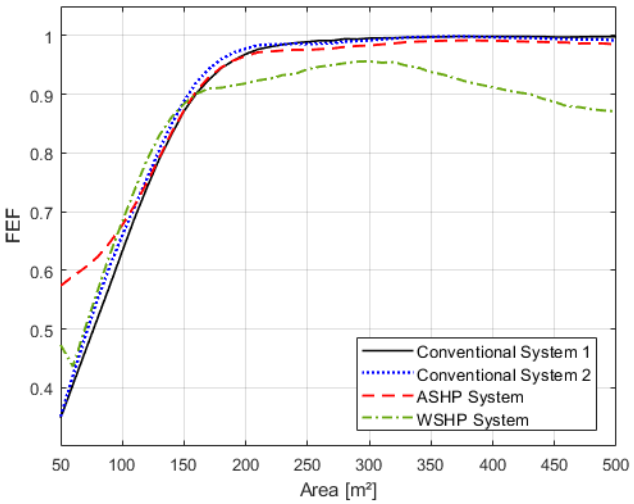

Figure 8: Comparison of the systems in terms of FEF versus installed solar collector area.

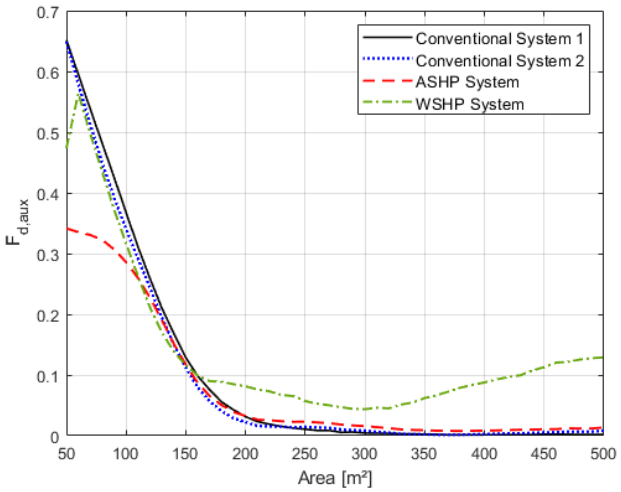

Figure 9: Comparison of the systems in terms of the fraction of demand for the auxiliary heater.

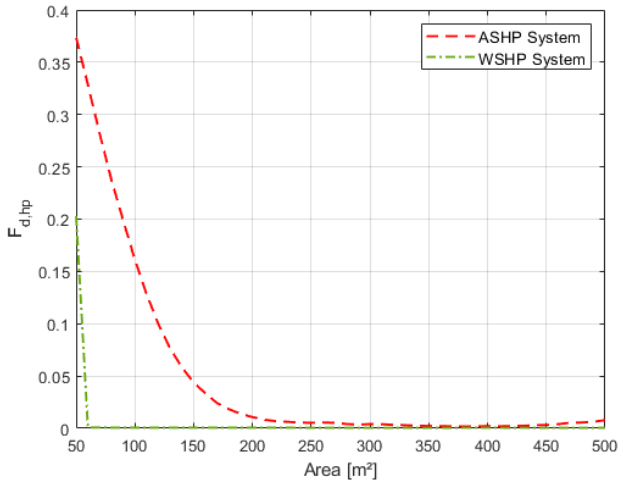

Figure 10: Comparison of the ASHP and WSHP systems in terms of the fraction of demand for the heat pump.

Conventional Systems 1 and 2 show similar curves overall, with the second one achieving higher FEF for areas between 150 and 200 m^2. This behaviour can be understood considering that the separation of the thermal storage in Conventional System 2 reduces the unwanted effect of destratification due to mixing within the tanks. However, at collector areas above 250 m^2 this benefit is overshadowed by the limited capacity of the fixed storage volumes. Therefore, Conventional System 1 surpasses all other configurations, with its variable storage volume capable of maintaing stratification at the increased heating capacities provided by the higher collector area.

Next, Fig. 9 shows the fraction of demand for the auxiliary heater, $F_{d,aux}$, for all four systems. For the combined

systems, this information is complemented by Fig. 10, which presents the fraction of demand for the heat pump, $F_{d,hp}$.

It may be observed that the best performance of the WSHP System occurs for a collector area of approximately 50 m^2, which corresponds to the range where this system's heat pump is capable of functioning. For all other areas, $F_{d,hp}$ remains approximately zero, indicating that the water temperatures are outside the heat pump's operating range. The ASHP System, however, shows the lowest values of $F_{d,aux}$ and the highest values of $F_{d,hp}$ between 50 and 150 m^2, when the heat pump complements the solar collectors. Above 200 m^2, the heat pump's operation becomes negligible. The Conventional Systems show values of $F_{d,aux}$ varying inversely to FEF in Fig. 8, which is expected since these configurations operate using only the collectors and auxiliary heater as heat sources.

6. CONCLUSION

The method used in this work consists of the implementation of mathematical models on MATLAB, using finite differences to explicitly solve differential and transient equations. The modeled systems were simulated over the period of one year, and the effect of varying the total solar collector area was studied. This form of analysis constitutes an accessible approach for simulating and analyzing transient solar water heating systems, since the software used is easily available and possesses an active user forum.

The results showed that all of the systems studied can be advantageous, depending on the area available for the instalation of solar collectors. For smaller areas, the system combined with an air source heat pump is the most efficient, whereas the first conventional configuration shows a superior performance for greater collector areas. The water source heat pump used in the other combined configuration, however, opperates only at a limited range of temperatures, which translates into poor applicability to the the location considered, in this case, the city of Natal - RN, Brazil, with high solar incidence and ambient temperatures.

Nevertheless, it is suggested that the theoretical model used for the thermal storage tanks be compared to an experimental analysis of the stratification phenomenon, in order to verify the simulated results. Additionally, the pattern of hot water consumption used in this work was taken from a study of a different location, which can potentially skew these results. Therefore, it is recommended that a future work considers consumption data obtained for the location in question.

7. ACKNOWLEDGEMENTS

The results of this work have been presented as part of the Bachelor's thesis of Fernandes (2018) for the degree of Graduate in Mechanical Engineering at the Federal University of Rio Grande do Norte, Natal, RN, on November 5, 2018.

8. REFERENCES

Cardemil, J.M. and Colle, S., 2010. "A base de dados SWERA como suporte para análises técnico-econômicas de plantas termo-solares". In *Anais do III Congresso Brasileiro de Energia Solar*. Belém, Brasil.

Duffie, J.A. and Beckman, W.A., 2006. *Solar Engineering of Thermal Processes*. John Wiley & Sons, New Jersey, 3rd edition.

Feister, U. and Grewe, R., 1995. "Spectral albedo measurements in the UV and visible region over different types of surfaces". *Photochemistry and photobiology*, Vol. 62, No. 4, pp. 736–744.

Fernandes, V.B., 2018. *Estudo técnico-ecônomico de sistemas solares combinados a bombas de calor para aquecimento de água*. Bachelor's thesis, Universidade Federal do Rio Grande do Norte, Natal, Brasil.

Freeman, T.L., Mitchell, J.W. and Audit, T.E., 1979. "Performance of combined solar-heat pump systems". *Solar Energy*, Vol. 22, pp. 125–135.

Gonçalves, J.E., 2016. *Análise de viabilidade técnic0-econômica de sistemas solares combinados a bombas de calor para aquecimento de água*. Master's thesis, Universidade Federal de Santa Catarina, Florianópolis, Brasil.

Naspolini, H.F., 2012. *Agregação da energia solar térmica ao aquecimento da água para o banho na moradia popular no Brasil.* Ph.D. thesis, Universidade Federal de Santa Catarina, Florianópolis, Brasil.

PROCEL, 2007. "Pesquisa de posse de equipamentos e hábitos de uso, ano base 2005: classe Residencial Relatório Brasil". ELETROBRAS; PROCEL, Rio de Janeiro, Brasil.

Salazar, J.P., 1997. *Economia de energia e redução do pico da curva de demanda para consumidores de baixa renda por agregação de energia solar térmica*. Master's thesis, Universidade Federal de Santa Catarina, Florianópolis, Brasil.

Sterling, S.J., 2011. *Feasibility analysis of two indirect heat pump assisted solar domestic hot water systems*. Master's thesis, University of Waterloo, Waterloo, Canada.

Welch, T., 2010. "Module 13: Design of air source heat pump systems for heating and hot water". CIBSE Journal. 20 Aug. 2018. <https://www.cibsejournal.com/cpd/modules/2010-02/>.

9. RESPONSIBILITY NOTICE

The authors are the only responsible for the printed material included in this paper.